Published in final edited form as:
*AJR Am J Roentgenol*. 2010 August ; 195(2): 292–300. doi:10.2214/AJR.10.4499.

# Assessment of Lung Inflammation With $^{18}$F-FDG PET During Acute Lung Injury

**Nicolas de Prost**, **Mauro R. Tucci**, and **Marcos F. Vidal Melo**
Department of Anesthesia, Critical Care, and Pain Medicine, Massachusetts General Hospital, 55 Fruit St., Boston, MA 02114

## Abstract

**Objective—**The purpose of this review is to describe the current experimental and clinical data regarding the fundamentals and applications of $^{18}$F-FDG PET during acute lung injury (ALI) and acute respiratory distress syndrome (ARDS).

**Conclusion—**Lung inflammation is a key feature of ALI. During ALI, FDG PET can be used to monitor lung neutrophils, which are essential cells in the pathophysiologic mechanisms of ALI. Pulmonary FDG kinetics are altered during experimental and human ALI and are associated with regional lung dysfunction, histologic abnormalities, and prognosis. FDG PET may be a valuable noninvasive method for gaining comprehensive understanding of the mechanisms of ALI/ARDS and for evaluating therapeutic interventions.

### Keywords

acute lung injury; acute respiratory distress syndrome; adults; $^{18}$F-FDG; PET

PET after IV administration of $^{18}$F-FDG has been used to study the global and regional metabolism of solid organs such as the brain and the heart [1–3] and has become a mainstay in oncology for diagnosis and treatment monitoring [4, 5]. Given that tissue FDG uptake is determined essentially by metabolic activity, it has also been used to study inflammation in nontumoral conditions [6, 7].

Acute lung injury (ALI) and acute respiratory distress syndrome (ARDS) are frequently encountered in critically ill patients and result in significant morbidity and mortality [8, 9]. Pulmonary inflammation is a key feature of both conditions and bears great relevance in their progress and resolution [10–12]. Accordingly, there is considerable interest in the application of FDG PET to ALI and ARDS because noninvasive and accurate quantification of pulmonary inflammation throughout the lung could be obtained, improving understanding of the disease mechanisms and assessment of therapeutic strategies. FDG PET also is an important advance over existing methods of studying lung inflammation. Open lung biopsy, the current reference standard, is invasive and restricted to the sampled region, and bronchoalveolar lavage, the less-invasive alternative, also is topographically limited [13]. In this review, we describe the current experimental and clinical data on the fundamentals and applications of FDG PET in ALI and ARDS.



Address correspondence to M. F. Vidal Melo (mvidalmelo@partners.org).

## ALI and ARDS

ALI is a clinical syndrome characterized by acute onset, infiltrates on chest radiographs, and hypoxemia ($PaO_2/F_iO_2$ ratio < 300 mm Hg) without an excessive increase in pulmonary capillary pressure [9, 14]. ARDS is the most severe form of ALI ($PaO_2/F_iO_2$ < 200 mm Hg). Both conditions can be the consequence of pulmonary or extrapulmonary insults [15, 16]. Increased alveolar capillary membrane permeability is a central feature of the acute phase of ALI and ARDS [17]. It is associated with diffuse alveolar damage, which includes alveolar flooding, infiltration by neutrophils and macrophages, and formation of hyaline membranes [12, 18]. The inflammatory process can evolve to a subacute phase characterized by fibroproliferation [10, 19]. Depending on the balance between fibroproliferation and alveolar repair, some patients recover without sequelae, but others experience pulmonary fibrosis and chronic respiratory failure [15, 20].

## Mechanisms of Lung FDG Uptake

### FDG Uptake by Cells

FDG is a glucose analogue used as a marker of glucose metabolism. It is transported into cells via the same GLUT family of transporter proteins as glucose (primarily GLUT-1). There, in the presence of hexokinase, it is phosphorylated to $^{18}$ F-FDG-6-phosphate, which unlike glucose-6-phosphate cannot be further metabolized via the Krebs cycle [21]. In tissues with low dephosphorylase activity (such as lung, brain, and heart) [22–26], dephosphorylation has been found to be negligible for at least 1 hour after FDG injection. FDG therefore is considered trapped intracellularly [26].

FDG is a biochemically active antimetabolite of glucose at concentrations several orders of magnitude greater than those encountered during in vivo clinical studies. This property seems negligible in clinical practice [27]. Indeed, cerebral glucose utilization measured with 6-$^{14}$C-glucose strongly correlates with $^{14}$C-deoxyglucose uptake ($r^2 = 0.97$) in various physiologic situations [28]. Understanding of the factors determining FDG uptake is crucial for adequate signal interpretation and introduction of FDG PET to clinical use.

### Neutrophils

Neutrophils become highly activated in response to inflammatory stimuli and are key modulators of the magnitude of injury during ALI and ARDS [29, 30]. They rely on anaerobic glycolysis for energy production and consume 20–30 times more glucose when activated than at rest [31]. The current concept, derived from experimental studies, is that the FDG imaging signal during ALI is predominantly determined by the combination of the absolute number of neutrophils in the field of view and their state of activation [32–35].

In rabbit models of pneumococcal pneumonia and bleomycin pneumonitis, autoradiography of histologic sections of lung after IV administration of $^{3}$H-deoxyglucose showed that deoxyglucose uptake was localized to neutrophils [34]. Regional instillation of complement component C5a and amorphous silica into rabbit lungs confirmed the specific localization of the signal to neutrophils [36]. The investigators also documented that neutrophil numbers in the lung were proportional to the FDG signal intensity after C5a instillation and pneumococcal pneumonia [35]. Lung FDG uptake has been associated with neutrophilic infiltration in a rat model of pancreatitis-associated lung injury [33]. During ventilator-induced lung injury in sheep, lung neutrophil counts were correlated with regional FDG uptake [35]. The same group found that this correlation persisted at the regional level in a sheep model of mild endotoxemia and heterogeneously distributed lung inflammation [37].

Neutrophil activation is characterized metabolically by an increase in glucose utilization per cell and, thus, increased FDG uptake. There are limited data on the biochemical determinants of FDG uptake by neutrophils. In an in vitro study [38], change in neutrophil shape, an early event after neutrophil activation [30], correlated best with metabolic activity. Surprisingly, neutrophil $^{3}$H-deoxyglucose uptake correlated with neither respiratory burst nor degranulation, two major processes in the neutrophil response to a bacterial insult [38].

Chen and Schuster [32] highlighted the relevance of the concept of neutrophil activation in determining FDG uptake. They found greater $^{3}$H-deoxyglucose uptake after IV administration of endotoxin than after administration of oleic acid for an equivalent number of bronchoalveolar lavage–harvested neutrophils in dogs [32]. Increased activation also was implied in a rat model of pancreatitisassociated lung injury in which changes in lung FDG uptake were larger than measurements of neutrophil accumulation or sequestration, such as myeloperoxidase activity and chemotactic peptide uptake [33].

Differences in activation also have been suggested in patients with bronchiectasis and pneumonia [39]. During pneumonia (more than 3 days after the onset of symptoms) high FDG uptake was associated with negligible lung influx of radiolabeled neutrophils, indicating high postmigratory activity of the accumulated inflammatory cells. In contrast, during bronchiectasis, FDG uptake was lower for substantial neutrophil influx, implying low metabolic activity of those cells [39].

## Other Inflammatory Cells

Neutrophil depletion experiments yielded evidence of the contribution of other cells to the FDG signal [35, 40]. Indeed, ALI and ARDS occur in neutropenic patients [41] and involve several types of inflammatory cells [42].

**Monocytes and macrophages—**Monocytes and macrophages are the first cells activated in various models of ALI [43, 44]. Moreover, in endotoxin models of ALI, the increase in macrophage counts is similar to [45, 46] or higher than [47] that of neutrophils. In other models of ALI, macrophage depletion has been found to protect the lung from dysfunction and injury [48–54]. Although macrophages take up FDG in atherosclerotic plaques [55–57] and in tumors [16], a $^{3}$H-deoxyglucose microautoradiographic study did not show any alveolar macrophage signal in acutely inflamed lung tissue [34]. This smaller contribution of macrophages to the FDG signal in acute lung states may be due to the inability of these cells to increase glucose uptake to the same extent as neutrophils do [58], despite the documented threefold increase in $^{3}$H-deoxyglucose uptake by peritoneal macrophages after infusion of lipopolysaccharide into mice [59].

**Lymphocytes—**Lymphocyte FDG uptake increases in vitro after activation [60]. However, FDG uptake during lung graft rejection, a predominantly T lymphocyte–mediated process, has been found similar to that in lung transplant recipients without rejection [61], suggesting a discrete contribution of lymphocytes to the FDG signal.

**Lung parenchymal cells—**The exact contribution of endothelial and epithelial cells to lung parenchymal FDG uptake during ALI and ARDS is unknown. That parenchymal cells contribute to the FDG signal is suggested by experimental data such as those obtained in a mouse model of ALI caused by endotoxin, in which lung FDG uptake decreased approximately one third with neutrophil depletion [40], implying that two thirds of uptake was due to other cells. In a sheep model of ventilator-induced lung injury, neutrophil depletion was associated with 70% reduction in FDG uptake [35]. Results of such studies not only support the concept that other cells contribute to the pulmonary FDG signal [35]

but also suggest that differences in lung parenchymal FDG uptake may occur and be associated with species differences and disease states [35, 40].

Endothelial cells are highly metabolically active [62, 63] and take up FDG after nitric oxide stimulation [64]. Regarding epithelial cells, the sodium–glucose cotransporter is a known key mechanism of lung metabolism and homeostasis at the apical membrane of alveolar epithelial cells, enhanced activity occurring when alveolar glucose concentration increases [65]. During ALI, plasma glucose enters the alveoli, a mechanism that suggests these cells also can contribute to FDG uptake.

## Methods of Quantifying FDG Uptake in the Lung

The simplest methods of quantifying pulmonary FDG are based on static indices such as the standardized uptake value (SUV) [66]. The interest in more accurate quantification of FDG uptake by lung parenchyma, not merely FDG activity in lung fields, led to the use of modeling methods. Models used to quantify FDG kinetics have been developed and validated mostly to study solid organs such as brain [2, 3], heart [1], and liver [67]. It has been recognized more recently, however, that specific models for studying pulmonary FDG kinetics, particularly in conditions of ALI, are required [68]. These models are needed because compared with solid organs, the lung has greater air content, lower basal glucose consumption [69], a larger perfusion to tissue ratio, and a larger parenchymal edema and flooding to tissue ratio during organ injury [70].

### Static Indices

Simplified quantitative measures that reflect raw FDG uptake have been developed in oncology because they are compatible with static whole-body FDG PET studies. Calculation of SUV is the most widely used method. The SUV represents FDG uptake within a region of interest (ROI) measured over a certain interval after FDG administration (typically > 45 minutes [71]) and normalized to the dose injected ($FDG_{dose}$) and to a body distribution factor such as body weight ($BW$). SUV is computed as follows:

$$SUV = AC_{ROI} / (FDG_{dose} / BW)$$

where $AC_{ROI}$ is the average activity concentration in the specified ROI. SUV quantification is affected by many factors reviewed elsewhere [71]. Among those, the main concern is that SUV encompasses blood and tissue activity within the studied ROI. As a result, intersubject and intrasubject variability in tissue blood volume contributes to the uncertainty of the SUV estimate. That SUV correlated poorly with dynamic indices in models of oleic acid– and endotoxin-induced lung injury in dogs [72] suggested that it was not suitable for quantifying FDG uptake during ALI.

In contrast, the tissue-to-plasma activity ratio, another static index, has been linearly correlated with the in vitro $^{3}$H-deoxyglucose uptake in that ALI model in dogs [72]. This index also was strongly correlated with dynamic indices [32], suggesting its usefulness in the quantification of FDG uptake. The tissue-to-plasma activity ratio is calculated by dividing the tissue activity data during the late imaging frames by the radioactivity in the plasma determined from the mean of two blood samples obtained at the end of that frame period [72]. However, the tissue-to-plasma activity ratio was not useful for discriminating patients with cystic fibrosis from healthy subjects [73], raising doubts on its clinical applicability.

Dual-time point scanning [74] is another static method useful for the diagnosis of malignancy [75] and assessment of idiopathic interstitial pneumonia [76], but to our knowledge it has not been studied in ALI.

## Dynamic Indices

Dynamic indices are derived from the kinetics of FDG, typically over a period of 60–75 minutes starting from the IV injection of the radiotracer [77–80]. Availability of these kinetic data together with plasma samples allows the fitting of compartmental models. These models are used to obtain estimates of variables related to FDG transport and uptake in tissue not only at the global organ level but also in specific ROIs. As in other applications [1–3], blood samples are drawn during imaging to determine the input function to the lung in the form of a plasma time–activity curve [81]. The following three compartmental models with an increasing number of compartments have been used to study pulmonary FDG kinetics during ALI.

**Two-compartment (Patlak) model—**Patlak et al. [2] proposed a model initially conceived to estimate cerebral glucose utilization. The model is composed of a central compartment in rapid equilibrium with blood plasma and a peripheral compartment in which the radiotracer is irreversibly trapped (Fig. 1). Patlak graphic analysis is based on an *xy*-plot on which the *y*-axis represents FDG activity in an ROI normalized to plasma activity and the *x*-axis is the integral of plasma activity in time normalized to plasma activity [2]. The net uptake rate (Patlak $K_i$[$K_{iP}$]) of the tissue under study is the slope of the straight portion of the curve, and the initial FDG distribution volume as a fraction of tissue volume ($V_e$) is the *y*-intercept of the linear regression (Fig. 2).

The main advantages of this model are simple application and interpretation. Jones et al. [39] proposed to express $K_{iP}$ normalized to $V_e$ to take into account the distribution volume of FDG in lung tissue. There is no reference standard and thus no agreement on this normalization, which significantly modifies the values of $K_{iP}$ in some cases [39, 82] but not others [79, 83]. Moreover, such normalization corrects for the amount of tissue in the ROI, but it is unknown whether it takes into account the lung edema/tissue ratio. This uncertainty is a major limitation of application of the Patlak model in ALI.

**Three-compartment (Sokoloff) model—**The three-compartment (Sokoloff) model was originally conceived to measure cerebral glucose uptake in rats [3] and subsequently in humans [84]. It has a blood and two tissue compartments, precursor and metabolic (Fig. 1). Transfer rates characterize the transport between compartments: $k_1$ quantifies facilitated FDG transport from blood into the tissue (precursor compartment) per unit of lung volume; $k_2$ quantifies tracer transport from the precursor compartment back into the blood; and $k_3$ characterizes FDG phosphorylation to $^{18}$F-FDG-6-phosphate (metabolic compartment), which is assumed to be proportional to hexokinase activity [3]. From these compartments, a global measure of the transfer rate of FDG from plasma to tissue ($K_{iS}$) and the distribution volume of the precursor compartment ($F_e$) as a fraction of lung volume can be computed:

$$K_{iS} = k_1 \times k_3/(k_2+k_3)$$
$$F_e = k_1/(k_2+k_3)$$

Thus

$$K_{iS} = F_e \times k_3$$

The Sokoloff model includes the assumptions that after phosphorylation the radiotracer is irreversibly trapped in the tissue and that all extravascular unmetabolized FDG in the region of interest is present in a single compartment, immediately available for hexokinase-mediated phosphorylation (precursor compartment). The latter assumption may be inaccurate for acutely injured lungs, in which large pools of edematous tissue can be functionally separated from cells trapping FDG. Therefore, the following compartment model specifically designed to reflect lung FDG kinetics during ALI has been developed [68].

**Four-compartment model—**The lung-specific four-compartment model was designed for the assessment of FDG kinetics in acutely inflamed lungs. It is aimed at situations in which pulmonary edema can increase the distribution volume of FDG. This model includes an extravascular and noncellular compartment in addition to blood and parenchyma and allows discrimination between the distribution volume of FDG that is a precursor for phosphorylation ($F_{ei}$, intracellular) and the volume that is not ($F_{ee}$, extracellular and noncellular). The rate constants $k_1$, $k_2$, and $k_3$ are the same as in the Sokoloff model. The rate constants $k_5$ and $k_6$ describe the changes in ROI activity concentration due to forward and backward FDG transfer between the precursor and the extravascular and noncellular compartments (Fig. 1). Thus in this model:

$$K_{iF} = F_{ei} \times k_3$$

Compared with the Sokoloff model, in which the Akaike information criterion (an index for quantifying quality of fit of a mathematic model, accounting for the number of parameters [85]) is used, the four-compartment model has yielded best fits in most injured lungs during ALI experiments [68]. The pulmonary FDG net uptake rate and distribution volume in the precursor pool for phosphorylation are correlated between the Sokoloff and the four-compartment models [68]. However, those variables were overestimated in the Sokoloff model (de Prost N et al., presented at the 2009 meeting of the American Society of Anesthesiologists). For all these reasons, the four-compartment lung-specific model seems best suited to describing FDG kinetics during ALI.

**Input function for compartmental modeling of FDG in the lung—**Assessment of lung FDG kinetics implies knowledge of the time–activity curve in pulmonary artery plasma as an input function. Acquisition of this input function typically involves sequential blood sampling, a process that is invasive and prone to measurement artifacts, exposes the clinical staff to radiation and blood, and adds costly laboratory procedures [86]. The lung input function can be estimated from a two-parameter model of the blood-pool ROI that accounts for partial-volume and spillover artifacts [81]. The method requires only two blood samples for calibration of the raw PET-derived blood activity data and yields estimates of FDG kinetics parameters highly correlated with blood samples [37, 68].

**Examples of FDG kinetics—**Regional FDG activity is influenced by the number of metabolically active cells, the activity of these cells, and the diffusion of radiotracer into edematous tissue [70]. Use of the described models allows identification of some of these factors. For instance, de Prost et al. (de Prost et al., 2009 ASA meeting) found in a sheep model of alveolar lavage that an increase in lung water can generate an additional volume of

distribution to FDG. This volume is not a precursor for phosphorylation and can artifactually increase lung FDG uptake independently of lung inflammation. Figure 3 illustrates this concept and shows the reduction of $K_i$ and of the estimates of the radiotracer distribution volume with the four-compartment model compared with the Sokoloff and Patlak models in a sheep model known to produce discrete inflammation and large alveolar flooding (saline lavage). In contrast, in states with larger contributions of inflammation, the increase in cell metabolism is the main determinant of $K_i$, and the values of $K_i$ produced by the four-compartment model are therefore close to those produced with the Sokoloff and Patlak models (Fig. 4).

## Use of FDG PET in Inflammatory Lung Diseases

### Pulmonary Infectious Diseases

FDG PET facilitates early visualization of lung infection in various experimental and clinical situations. Using a rabbit model of *Streptococcus pneumoniae* pneumonia [34], Jones et al. found that lung FDG uptake was pronounced 15 hours after instillation of bacteria but had decreased to almost baseline values 48 hours after instillation [39]. In healthy subjects receiving a moderate local lung instillation of endotoxin, FDG PET can depict inflammation, suggesting its sensitivity in quantifying the early phase of an acute inflammatory response [79]. FDG PET also has been used to measure the effect of antiinflammatory interventions, suggesting its applicability in the testing of novel drugs [83]. The clinical value of lung FDG uptake has been exemplified in cystic fibrosis patients with no sign of acute infectious exacerbation. The magnitude of uptake was associated with the speed of decline in pulmonary function [73].

### Subacute and Chronic Lung Inflammatory Diseases

In a rabbit model of pulmonary fibrosis [36], the FDG signal intensity increased and stayed high for as long as 4 weeks after administration of fibrogenic agents; the signal was predominantly derived from neutrophils. A 2009 study [87] showed that in patients with pulmonary fibrosis, the highest FDG PET SUVs coregistered with high-resolution CT patterns, such as honeycombing, which is classically understood as representative of irreversible parenchymal scarring. The authors hypothesized that this finding reflected high fibroblastic activity, suggesting an opportunity for pharmacologic manipulation.

Applications of FDG PET in the assessment of airway inflammation have resulted in higher FDG uptake in persons with chronic COPD than in those with asthma [82]. Although both groups had high sputum neutrophil counts, this count correlated with FDG uptake only in COPD patients, implying a difference in neutrophil status. This finding suggests that FDG PET provides a potentially important marker of persistent lung inflammation.

### Experimental Acute Lung Injury

**Smoke inhalation—**Schroeder et al. [80] found a significant and early (2 hours) increase in regional FDG uptake in sheep lungs acutely exposed to smoke inhalation. Regional FDG uptake (Fig. 5) appeared to be predictive of regional gas exchange impairment in this model, suggesting a function–inflammation relation. The findings also suggested a direct association between the degree of ventilation– perfusion heterogeneity before injury and the postinjury magnitude of FDG uptake.

**Ventilator-induced lung injury—**Musch et al. [35] found that increased regional FDG uptake exclusively due to mechanical forces can be detected in a sheep model of ventilator-induced lung injury after only 90 minutes of mechanical ventilation. When positive end-expiratory pressure was associated with overdistention, increased FDG uptake was observed

and associated with mild neutrophil infiltration despite the absence of impairment of gas exchange and respiratory system compliance, suggesting that the FDG signal preceded regional dysfunction (Fig. 6). The combination of overdistention with lung collapse led to a marked increase in FDG uptake, marked regional gas exchange and mechanical dysfunction, and pronounced neutrophilic infiltration.

**Endotoxemia—**Using the Sokoloff model, Costa et al. [37] found that FDG PET can be used to detect early regional cellular activation during mild endotoxemia associated with a moderately aggressive mode of ventilation (Fig. 7). Moreover, heterogeneous lung aeration due to mechanical ventilation of the supine lungs with large tidal expansion produced spatially heterogeneous FDG uptake associated with heterogeneous pulmonary neutrophilic infiltration.

### Clinical Acute Lung Injury

**Traumatic lung injury—**Addressing the predictive value of FDG PET, Rodrigues et al. [88] conducted a study with eight patients with pulmonary contusion, none initially meeting the criteria for ARDS. At FDG PET 24–72 hours after admission, three of the four patients in whom ARDS developed had diffuse FDG uptake throughout the lungs (Fig. 8A), but all four of the patients in whom ARDS did not develop had significant FDG uptake only in areas of focal lung opacity on CT images (Fig. 8B). The SUV of the normally aerated lung was higher in patients with ARDS than in those in whom ARDS did not develop, suggesting that FDG PET provides valuable predictive information during the early stages of ALI.

**ARDS—**Bellani et al. [77] studied the distribution of FDG uptake, as measured with $K_{iP}$, in the lungs of patients with established ARDS. Those investigators found that the relation between FDG uptake and lung density followed two different patterns. In seven patients, $K_{iP}$ was highest in regions with the highest density, and in three patients, $K_{iP}$ was higher in normally or poorly aerated regions than in nonaerated regions. This finding suggests that aerated regions (so-called baby lung) can be considerably infiltrated with inflammatory cells and emphasizes the great potential of FDG PET for noninvasive exploration of the relations between structure, function, and inflammation in ALI and ARDS.

## Conclusion

In the acutely inflamed lung, FDG PET facilitates noninvasive assessment of regional lung neutrophil infiltration and activation. This ability has led to considerable improvement in the experimental and clinical pathophysiologic investigation of ALI and ARDS. To our knowledge, lung-specific compartmental models that account for the presence of an extracellular compartment have never been used in humans. Results of animal studies suggest use of these models may improve quantification of the FDG signal in ALI and ARDS. Further research is needed to explore the biologic correlates of FDG uptake. Better understanding of such mechanisms is required before FDG PET can be used as a decision-making tool in the treatment of patients with ALI and ARDS.

## Acknowledgments

The authors thank Kathryn Morton, Department of Radiology, University of Utah School of Medicine, for providing FDG PET images of trauma patients.

Supported by NIH grant HL 5R01HL086827. N. de Prost received a scholarship from LEEM Recherche and the Société de Pneumologie de Langue Française. M. R. Tucci received a scholarship from CAPES (Brazilian Ministry of Education).

## References


1. Ghesani M, Depuey EG, Rozanski A. Role of F-18 FDG positron emission tomography (PET) in the assessment of myocardial viability. Echocardiography. 2005; 22:165–177. [PubMed: 15693785]
2. Patlak CS, Blasberg RG, Fenstermacher JD. Graphical evaluation of blood-to-brain transfer constants from multiple-time uptake data. J Cereb Blood Flow Metab. 1983; 3:1–7. [PubMed: 6822610]
3. Sokoloff L, Reivich M, Kennedy C, et al. The [$^{14}$C] deoxyglucose method for the measurement of local cerebral glucose utilization: theory, procedure, and normal values in the conscious and anesthetized albino rat. J Neurochem. 1977; 28:897–916. [PubMed: 864466]
4. Gould MK, Maclean CC, Kuschner WG, Rydzak CE, Owens DK. Accuracy of positron emission tomography for diagnosis of pulmonary nodules and mass lesions: a meta-analysis. JAMA. 2001; 285:914–924. [PubMed: 11180735]
5. Bury T, Corhay JL, Duysinx B, et al. Value of FDG-PET in detecting residual or recurrent nonsmall cell lung cancer. Eur Respir J. 1999; 14:1376–1380. [PubMed: 10624770]
6. Keidar Z, Gurman-Balbir A, Gaitini D, Israel O. Fever of unknown origin: the role of $^{18}$F-FDG PET/CT. J Nucl Med. 2008; 49:1980–1985. [PubMed: 18997040]
7. Jones HA. Inflammation imaging. Proc Am Thorac Soc. 2005; 2:513–544. 545–548.
8. Ashbaugh DG, Bigelow DB, Petty TL, Levine BE. Acute respiratory distress in adults. Lancet. 1967; 2:319–323. [PubMed: 4143721]
9. Bernard GR, Artigas A, Brigham KL, et al. The American-European Consensus Conference on ARDS: definitions, mechanisms, relevant outcomes, and clinical trial coordination. Am J Respir Crit Care Med. 1994; 149:818–824. [PubMed: 7509706]
10. Ware LB, Matthay MA. The acute respiratory distress syndrome. N Engl J Med. 2000; 342:1334–1349. [PubMed: 10793167]
11. Park WY, Goodman RB, Steinberg KP, et al. Cytokine balance in the lungs of patients with acute respiratory distress syndrome. Am J Respir Crit Care Med. 2001; 164:1896–1903. [PubMed: 11734443]
12. Anderson WR, Thielen K. Correlative study of adult respiratory distress syndrome by light, scanning, and transmission electron microscopy. Ultrastruct Pathol. 1992; 16:615–628. [PubMed: 1448881]
13. Rhodes CG, Hughes JM. Pulmonary studies using positron emission tomography. Eur Respir J. 1995; 8:1001–1017. [PubMed: 7589363]
14. Slutsky AS. Consensus conference on mechanical ventilation—January 28–30, 1993 at Northbrook, Illinois, USA. Part I. European Society of Intensive Care Medicine, the ACCP and the SCCM. Intensive Care Med. 1994; 20:64–79. [PubMed: 8163765]
15. Barth PJ, Holtermann W, Muller B. The spatial distribution of pulmonary lesions in severe ARDS: an autopsy study of 35 cases. Pathol Res Pract. 1998; 194:465–471. [PubMed: 9728363]
16. Kubota R, Yamada S, Kubota K, Ishiwata K, Tamahashi N, Ido T. Intratumoral distribution of fluorine-18-fluorodeoxyglucose in vivo: high accumulation in macrophages and granulation tissues studied by microautoradiography. J Nucl Med. 1992; 33:1972–1980. [PubMed: 1432158]
17. Wang HM, Bodenstein M, Markstaller K. Overview of the pathology of three widely used animal models of acute lung injury. Eur Surg Res. 2008; 40:305–316. [PubMed: 18349543]
18. Penuelas O, Aramburu JA, Frutos-Vivar F, Esteban A. Pathology of acute lung injury and acute respiratory distress syndrome: a clinical–pathological correlation. Clin Chest Med. 2006; 27:571–578. [PubMed: 17085246]
19. Marshall RP, Bellingan G, Webb S, et al. Fibroproliferation occurs early in the acute respiratory distress syndrome and impacts on outcome. Am J Respir Crit Care Med. 2000; 162:1783–1788. [PubMed: 11069813]
20. Steinberg KP, Hudson LD, Goodman RB, et al. Efficacy and safety of corticosteroids for persistent acute respiratory distress syndrome. N Engl J Med. 2006; 354:1671–1684. [PubMed: 16625008]
21. Pauwels EK, Sturm EJ, Bombardieri E, Cleton FJ, Stokkel MP. Positron-emission tomography with [$^{18}$F]fluorodeoxyglucose. Part 1. Biochemical uptake mechanism and its implication for clinical studies. J Cancer Res Clin Oncol. 2000; 126:549–559. [PubMed: 11043392]

22. Weber G, Cantero A. Glucose-6-phosphatase activity in normal, precancerous and neoplastic tissues. Cancer Res. 1955; 15:105–108. [PubMed: 14352196]
23. Phelps ME, Huang SC, Hoffman EJ, Selin C, Sokoloff L, Kuhl DE. Tomographic measurement of local cerebral glucose metabolic rate in humans with (F-18)2-fluoro-2-deoxy-D-glucose: validation of method. Ann Neurol. 1979; 6:371–388. [PubMed: 117743]
24. Nelson CA, Wang JQ, Leav I, Crane PD. The interaction among glucose transport, hexokinase, and glucose-6-phosphatase with respect to $^{3}$H-2-deoxyglucose retention in murine tumor models. Nucl Med Biol. 1996; 23:533–541. [PubMed: 8832712]
25. Spence AM, Muzi M, Mankoff DA, et al. $^{18}$F-FDG PET of gliomas at delayed intervals: improved distinction between tumor and normal gray matter. J Nucl Med. 2004; 45:1653–1659. [PubMed: 15471829]
26. Gallagher BM, Fowler JS, Gutterson NI, MacGregor RR, Wan CN, Wolf AP. Metabolic trapping as a principle of radiopharmaceutical design: some factors responsible for the biodistribution of [$^{18}$F] 2-deoxy-2-fluoro-D-glucose. J Nucl Med. 1978; 19:1154–1161. [PubMed: 214528]
27. Wiebe LI. FDG metabolism: quaecumque sunt vera. J Nucl Med. 2001; 42:1679–1681. [PubMed: 11696639]
28. Collins RC, McCandless DW, Wagman IL. Cerebral glucose utilization: comparison of [$^{14}$C]deoxyglucose and [6-$^{14}$C]glucose quantitative autoradiography. J Neurochem. 1987; 49:1564–1570. [PubMed: 3668540]
29. Azoulay E, Attalah H, Yang K, et al. Exacerbation with granulocyte colony-stimulating factor of prior acute lung injury during neutropenia recovery in rats. Crit Care Med. 2003; 31:157–165. [PubMed: 12545010]
30. Hogg JC. Neutrophil kinetics and lung injury. Physiol Rev. 1987; 67:1249–1295. [PubMed: 3317458]
31. McCall CE, Bass DA, Cousart S, DeChatelet LR. Enhancement of hexose uptake in human polymorphonuclear leukocytes by activated complement component C5a. Proc Natl Acad Sci USA. 1979; 76:5896–5900. [PubMed: 293691]
32. Chen DL, Schuster DP. Positron emission tomography with [$^{18}$F]fluorodeoxyglucose to evaluate neutrophil kinetics during acute lung injury. Am J Physiol Lung Cell Mol Physiol. 2004; 286:L834–L840. [PubMed: 14660487]
33. Hartwig W, Carter EA, Jimenez RE, et al. Neutrophil metabolic activity but not neutrophil sequestration reflects the development of pancreatitis-associated lung injury. Crit Care Med. 2002; 30:2075–2082. [PubMed: 12352044]
34. Jones HA, Clark RJ, Rhodes CG, Schofield JB, Krausz T, Haslett C. In vivo measurement of neutrophil activity in experimental lung inflammation. Am J Respir Crit Care Med. 1994; 149:1635–1639. [PubMed: 7516252]
35. Musch G, Venegas JG, Bellani G, et al. Regional gas exchange and cellular metabolic activity in ventilator-induced lung injury. Anesthesiology. 2007; 106:723–735. [PubMed: 17413910]
36. Jones HA, Schofield JB, Krausz T, Boobis AR, Haslett C. Pulmonary fibrosis correlates with duration of tissue neutrophil activation. Am J Respir Crit Care Med. 1998; 158:620–628. [PubMed: 9700143]
37. Costa EL, Musch G, Winkler T, et al. Mild endotoxemia during mechanical ventilation produces spatially heterogeneous pulmonary neutrophilic inflammation in sheep. Anesthesiology. 2010; 112:658–669. [PubMed: 20179503]
38. Jones HA, Cadwallader KA, White JF, Uddin M, Peters AM, Chilvers ER. Dissociation between respiratory burst activity and deoxyglucose uptake in human neutrophil granulocytes: implications for interpretation of (18)F-FDG PET images. J Nucl Med. 2002; 43:652–657. [PubMed: 11994530]
39. Jones HA, Sriskandan S, Peters AM, et al. Dissociation of neutrophil emigration and metabolic activity in lobar pneumonia and bronchiectasis. Eur Respir J. 1997; 10:795–803. [PubMed: 9150315]
40. Zhou Z, Kozlowski J, Goodrich AL, Markman N, Chen DL, Schuster DP. Molecular imaging of lung glucose uptake after endotoxin in mice. Am J Physiol Lung Cell Mol Physiol. 2005; 289:L760–L768. [PubMed: 15980036]

41. Ognibene FP, Martin SE, Parker MM, et al. Adult respiratory distress syndrome in patients with severe neutropenia. N Engl J Med. 1986; 315:547–551. [PubMed: 3736638]
42. Matthay MA, Zimmerman GA. Acute lung injury and the acute respiratory distress syndrome: four decades of inquiry into pathogenesis and rational management. Am J Respir Cell Mol Biol. 2005; 33:319–327. [PubMed: 16172252]
43. Gattinoni L, Carlesso E, Cadringher P, Valenza F, Vagginelli F, Chiumello D. Physical and biological triggers of ventilator-induced lung injury and its prevention. Eur Respir J Suppl. 2003; 47:15s–25s. [PubMed: 14621113]
44. Suratt BT, Parsons PE. Mechanisms of acute lung injury/acute respiratory distress syndrome. Clin Chest Med. 2006; 27:579–589. [PubMed: 17085247]
45. Ohgami M, Doerschuk CM, Gie RP, English D, Hogg JC. Late effects of endotoxin on the accumulation and function of monocytes in rabbit lungs. Am Rev Respir Dis. 1992; 146:190–195. [PubMed: 1626802]
46. Nakagawa M, Ohgami M, Ando N, Wakabayashi G, Kitajima M. Effects of steroids on the lung accumulation of neutrophil and monocyte in rabbits with endotoxemia. Chest. 1996; 109:1339–1345. [PubMed: 8625688]
47. Wang CZ, Herndon DN, Traber LD, et al. Pulmonary inflammatory cell response to sustained endotoxin administration. J Appl Physiol. 1994; 76:516–522. [PubMed: 8175557]
48. Zhao M, Fernandez LG, Doctor A, et al. Alveolar macrophage activation is a key initiation signal for acute lung ischemia-reperfusion injury. Am J Physiol Lung Cell Mol Physiol. 2006; 291:L1018–L1026. [PubMed: 16861385]
49. O'Dea KP, Young AJ, Yamamoto H, Robotham JL, Brennan FM, Takata M. Lung-marginated monocytes modulate pulmonary microvascular injury during early endotoxemia. Am J Respir Crit Care Med. 2005; 172:1119–1127. [PubMed: 16081546]
50. Parbhakar OP, Duke T, Townsend HG, Singh B. Depletion of pulmonary intravascular macrophages partially inhibits lipopolysaccharide-induced lung inflammation in horses. Vet Res. 2005; 36:557–569. [PubMed: 15955281]
51. Singh B, Pearce JW, Gamage LN, Janardhan K, Caldwell S. Depletion of pulmonary intravascular macrophages inhibits acute lung inflammation. Am J Physiol Lung Cell Mol Physiol. 2004; 286:L363–L372. [PubMed: 14565942]
52. Standiford TJ, Kunkel SL, Lukacs NW, et al. Macrophage inflammatory protein-1 alpha mediates lung leukocyte recruitment, lung capillary leak, and early mortality in murine endotoxemia. J Immunol. 1995; 155:1515–1524. [PubMed: 7636213]
53. Sone Y, Serikov VB, Staub NC Sr. Intravascular macrophage depletion attenuates endotoxin lung injury in anesthetized sheep. J Appl Physiol. 1999; 87:1354–1359. [PubMed: 10517763]
54. Gaca JG, Palestrant D, Lukes DJ, Olausson M, Parker W, Davis RD Jr. Prevention of acute lung injury in swine: depletion of pulmonary intravascular macrophages using liposomal clodronate. J Surg Res. 2003; 112:19–25. [PubMed: 12873428]
55. Hyafil F, Cornily JC, Rudd JH, Machac J, Feldman LJ, Fayad ZA. Quantification of inflammation within rabbit atherosclerotic plaques using the macrophage-specific CT contrast agent N1177: a comparison with $^{18}$F-FDG PET/CT and histology. J Nucl Med. 2009; 50:959–965. [PubMed: 19443582]
56. Nahrendorf M, Zhang H, Hembrador S, et al. Nanoparticle PET-CT imaging of macrophages in inflammatory atherosclerosis. Circulation. 2008; 117:379–387. [PubMed: 18158358]
57. Ogawa M, Ishino S, Mukai T, et al. (18)F-FDG accumulation in atherosclerotic plaques: immunohistochemical and PET imaging study. J Nucl Med. 2004; 45:1245–1250. [PubMed: 15235073]
58. Reiss M, Roos D. Differences in oxygen metabolism of phagocytosing monocytes and neutrophils. J Clin Invest. 1978; 61:480–488. [PubMed: 202614]
59. Gamelli RL, Liu H, He LK, Hofmann CA. Augmentations of glucose uptake and glucose transporter-1 in macrophages following thermal injury and sepsis in mice. J Leukoc Biol. 1996; 59:639–647. [PubMed: 8656048]

60. Ishimori T, Saga T, Mamede M, et al. Increased (18)F-FDG uptake in a model of inflammation: concanavalin A-mediated lymphocyte activation. J Nucl Med. 2002; 43:658–663. [PubMed: 11994531]
61. Jones HA, Donovan T, Goddard MJ, et al. Use of 18FDG-PET to discriminate between infection and rejection in lung transplant recipients. Transplantation. 2004; 77:1462–1464. [PubMed: 15167609]
62. Maschauer S, Prante O, Hoffmann M, Deichen JT, Kuwert T. Characterization of $^{18}$F-FDG uptake in human endothelial cells in vitro. J Nucl Med. 2004; 45:455–460. [PubMed: 15001687]
63. Buck AK, Reske SN. Cellular origin and molecular mechanisms of $^{18}$F-FDG uptake: is there a contribution of the endothelium? J Nucl Med. 2004; 45:461–463. [PubMed: 15001688]
64. Paik JY, Lee KH, Ko BH, Choe YS, Choi Y, Kim BT. Nitric oxide stimulates $^{18}$F-FDG uptake in human endothelial cells through increased hexokinase activity and GLUT1 expression. J Nucl Med. 2005; 46:365–370. [PubMed: 15695798]
65. de Prost N, Saumon G. Glucose transport in the lung and its role in liquid movement. Respir Physiol Neurobiol. 2007; 159:331–337. [PubMed: 17369109]
66. Sadato N, Tsuchida T, Nakaumra S, et al. Non-invasive estimation of the net influx constant using the standardized uptake value for quantification of FDG uptake of tumours. Eur J Nucl Med. 1998; 25:559–564. [PubMed: 9618569]
67. Choi Y, Hawkins RA, Huang SC, et al. Evaluation of the effect of glucose ingestion and kinetic model configurations of FDG in the normal liver. J Nucl Med. 1994; 35:818–823. [PubMed: 8176464]
68. Schroeder T, Vidal Melo MF, Musch G, Harris RS, Venegas JG, Winkler T. Modeling pulmonary kinetics of 2-deoxy-2-[18F]fluoro-D-glucose during acute lung injury. Acad Radiol. 2008; 15:763–775. [PubMed: 18486012]
69. Paquet N, Albert A, Foidart J, Hustinx R. Within-patient variability of (18)F-FDG: standardized uptake values in normal tissues. J Nucl Med. 2004; 45:784–788. [PubMed: 15136627]
70. Hedlund LW, Vock P, Effmann EL, Lischko MM, Putman CE. Hydrostatic pulmonary edema: an analysis of lung density changes by computed tomography. Invest Radiol. 1984; 19:254–262. [PubMed: 6480302]
71. Boellaard R. Standards for PET image acquisition and quantitative data analysis. J Nucl Med. 2009; 50(suppl 1):11S–20S. [PubMed: 19380405]
72. Chen DL, Mintun MA, Schuster DP. Comparison of methods to quantitate $^{18}$F-FDG uptake with PET during experimental acute lung injury. J Nucl Med. 2004; 45:1583–1590. [PubMed: 15347728]
73. Chen DL, Ferkol TW, Mintun MA, Pittman JE, Rosenbluth DB, Schuster DP. Quantifying pulmonary inflammation in cystic fibrosis with positron emission tomography. Am J Respir Crit Care Med. 2006; 173:1363–1369. [PubMed: 16543553]
74. Zhuang H, Pourdehnad M, Lambright ES, et al. Dual time point $^{18}$F-FDG PET imaging for differentiating malignant from inflammatory processes. J Nucl Med. 2001; 42:1412–1417. [PubMed: 11535734]
75. Basu S, Alavi A. Partial volume correction of standardized uptake values and the dual time point in FDG-PET imaging: should these be routinely employed in assessing patients with cancer? Eur J Nucl Med Mol Imaging. 2007; 34:1527–1529. [PubMed: 17522857]
76. Umeda Y, Demura Y, Ishizaki T, et al. Dual-time-point $^{18}$F-FDG PET imaging for diagnosis of disease type and disease activity in patients with idiopathic interstitial pneumonia. Eur J Nucl Med Mol Imaging. 2009; 36:1121–1130. [PubMed: 19247654]
77. Bellani G, Messa C, Guerra L, et al. Lungs of patients with acute respiratory distress syndrome show diffuse inflammation in normally aerated regions: a [18F]-fluoro-2-deoxy-D-glucose PET/CT study. Crit Care Med. 2009; 37:2216–2222. [PubMed: 19487931]
78. Chen DL, Richard JC, Schuster DP. Molecular imaging of enzyme function in lungs. Methods Enzymol. 2004; 385:315–333. [PubMed: 15130746]
79. Chen DL, Rosenbluth DB, Mintun MA, Schuster DP. FDG-PET imaging of pulmonary inflammation in healthy volunteers after airway instillation of endotoxin. J Appl Physiol. 2006; 100:1602–1609. [PubMed: 16424067]

80. Schroeder T, Vidal Melo MF, Musch G, Harris RS, Winkler T, Venegas JG. PET imaging of regional 18F-FDG uptake and lung function after cigarette smoke inhalation. J Nucl Med. 2007; 48:413–419. [PubMed: 17332619]
81. Schroeder T, Vidal Melo MF, Musch G, Harris RS, Venegas JG, Winkler T. Image-derived input function for assessment of 18F-FDG uptake by the inflamed lung. J Nucl Med. 2007; 48:1889–1896. [PubMed: 17942803]
82. Jones HA, Marino PS, Shakur BH, Morrell NW. In vivo assessment of lung inflammatory cell activity in patients with COPD and asthma. Eur Respir J. 2003; 21:567–573. [PubMed: 12762337]
83. Chen DL, Bedient TJ, Kozlowski J, et al. [$^{18}$F]fluorodeoxyglucose positron emission tomography for lung antiinflammatory response evaluation. Am J Respir Crit Care Med. 2009; 180:533–539. [PubMed: 19574441]
84. Reivich M, Kuhl D, Wolf A, et al. The [$^{18}$F]fluorodeoxyglucose method for the measurement of local cerebral glucose utilization in man. Circ Res. 1979; 44:127–137. [PubMed: 363301]
85. Landaw EM, DiStefano JJ 3rd. Multiexponential, multicompartmental, and noncompartmental modeling. Part 2. Data analysis and statistical considerations. Am J Physiol. 1984; 246:R665–R677. [PubMed: 6720989]
86. Wong WH, Hicks K. A clinically practical method to acquire parametric images of unidirectional metabolic rates and blood spaces. J Nucl Med. 1994; 35:1206–1212. [PubMed: 8014684]
87. Groves AM, Win T, Screaton NJ, et al. Idiopathic pulmonary fibrosis and diffuse parenchymal lung disease: implications from initial experience with $^{18}$F-FDG PET/CT. J Nucl Med. 2009; 50:538–545. [PubMed: 19289428]
88. Rodrigues RS, Miller PR, Bozza FA, et al. FDG-PET in patients at risk for acute respiratory distress syndrome: a preliminary report. Intensive Care Med. 2008; 34:2273–2278. [PubMed: 18682917]

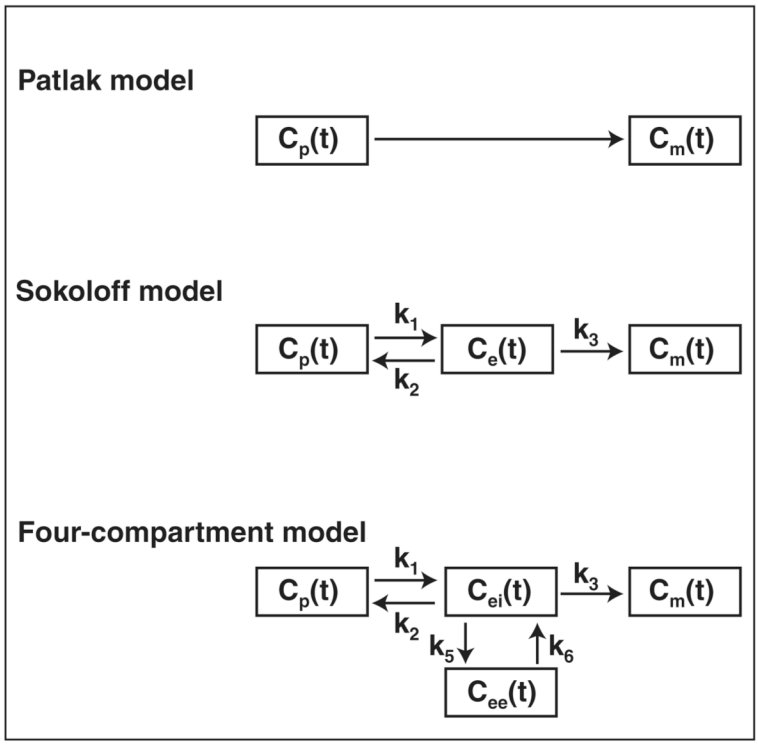


**Fig. 1.**

Tracer kinetic models of $^{18}$F-FDG: generalized two-compartment (Patlak), three-compartment (Sokoloff) model, and lung-specific four-compartment model, which includes two equilibrating compartments. Arrows indicate directions of mass transport. $C_p(t)$ = activity concentration of FDG in plasma; $C_e(t)$ and $C_{ei}(t)$ = FDG concentrations in extravascular compartment serving as substrate pool for hexokinase in Sokoloff ($C_e$) and in four-compartment ($C_{ei}$) models, $C_{ee}(t)$ = FDG concentration in extravascular or noncellular compartment, $C_m(t)$ = concentration of phosphorylated FDG. Rate constants $k_1$ and $k_2$ account for forward and backward transport of FDG between blood and tissue; $k_3$ is rate of FDG phosphorylation; $k_5$ and $k_6$ account for forward and backward transport of FDG between substrate (intracellular) and nonsubstrate (extracellular) compartments.

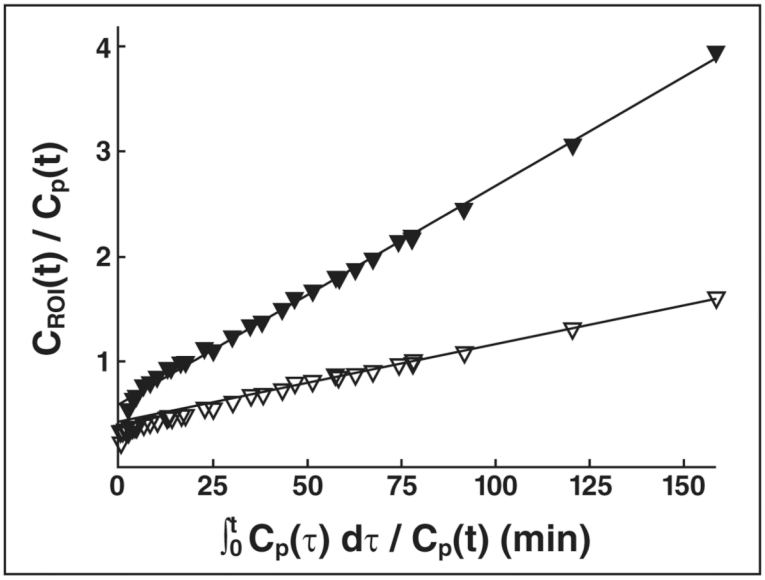


**Fig. 2.**

Patlak plots for lung subjected to aggressive ventilation strategy (peak inspiratory pressure, 50 cm $H_2O$; end-expiratory pressure, −10 cm $H_2O$) (*solid triangles*) and lung protected from aggressive mechanical ventilation (*open triangles*). Plots represent $^{18}$F-FDG activity in region of interest ($C_{ROI}$) normalized to plasma activity ($C_p$) versus integral of plasma activity normalized to plasma activity. FDG uptake rate, calculated as slope of linear portion of plot, is higher in lung subjected to aggressive mechanical ventilation. (Reprinted with permission from [35])

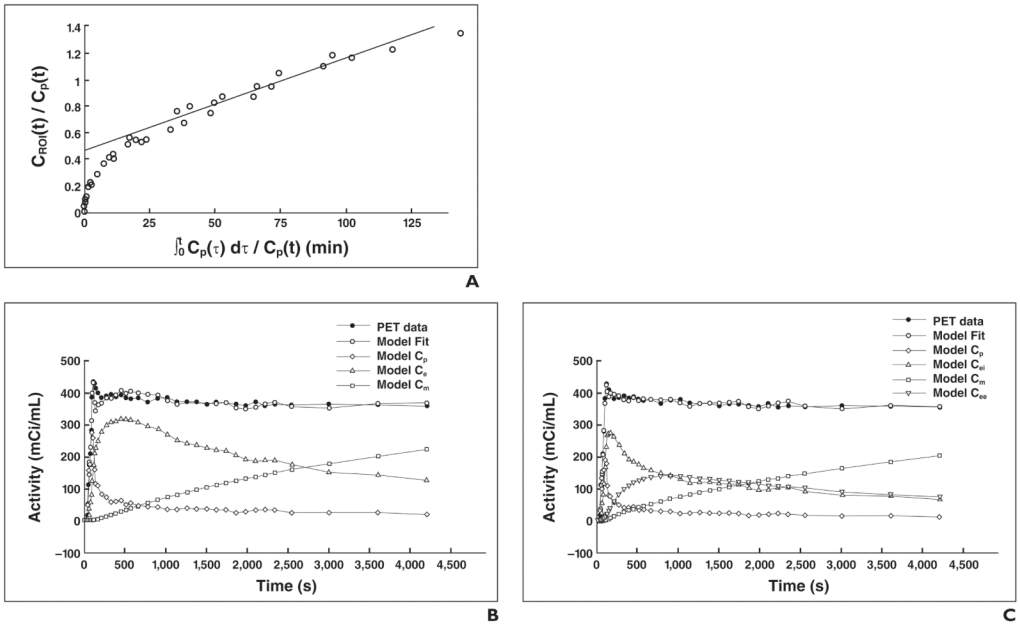


**Fig. 3.**

Modeling of kinetics of $^{18}$F-FDG in dependent region of sheep lung subjected to surfactant depletion with saline lavage in three kinetics models. $C_p$ = activity concentration of FDG in plasma; $C_e$ and $C_{ei}$ = region of interest (ROI) concentrations of extravascular FDG serving as substrate pool for hexokinase in Sokoloff and four-compartment models, respectively; $C_{ee}$ = ROI concentration of FDG in extravascular and noncellular compartment; $C_m$ = ROI concentration of phosphorylated FDG.

**A,** Patlak model. $K_{iP}$ = 0.0071/min, *y*-intercept = 0.46 (Patlak equation, $y = 0.0071x + 0.46$). $C_{ROI}$ = $^{18}$F-FDG activity in region of interest.

**B,** Sokoloff model. $K_{iS}$ = 0.0051/min, $k_3$ = 0.0159/min, and $F_e$ = 0.32 ($K_{iS} = k_3 \times F_e$).

**C,** Four-compartment model. $K_{iF}$ = 0.0046/min, $k_3$ = 0.0260/min, $F_{ei}$ = 0.1786, and $F_{ee}$ = 0.1769 ($K_{iF} = k_3 \times F_{ei}$). $K_{iF} < K_{iS}$, and $K_{iP}$, and $F_{ei} < F_e$ and Patlak *y*-intercept. This last result shows that use of four-compartment model leads to smaller size of compartment that is direct precursor for phosphorylation than in Patlak and Sokoloff models. This reduction in estimates of precursor volume accompanies reduction in estimates of net FDG uptake rate $K_i$.

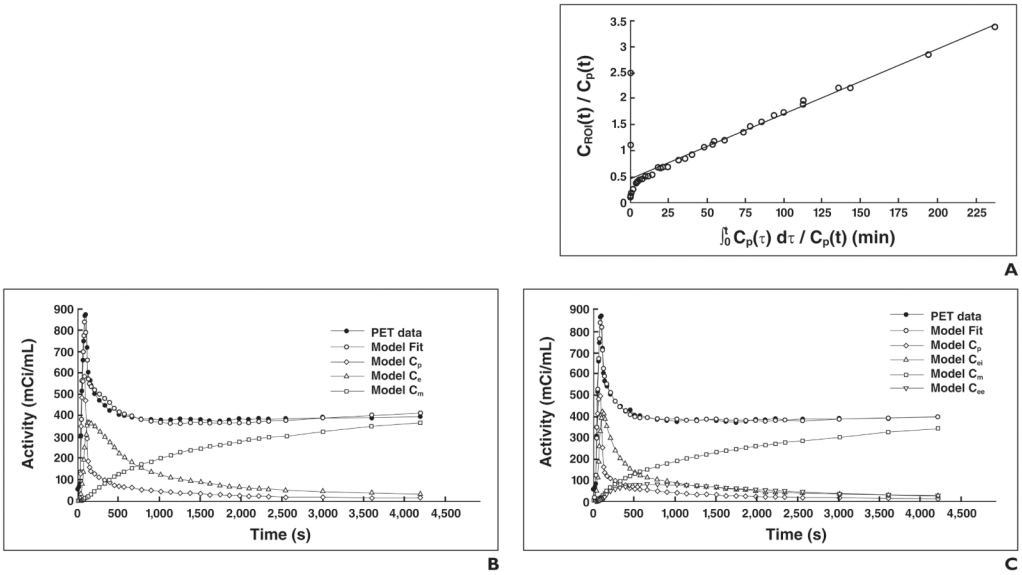


**Fig. 4.**

Modeling of kinetics of $^{18}$F-FDG in dependent region of normal sheep lung after administration of 2-hour infusion of endotoxin (10 ng/kg/min) in three kinetics models. $Ki_F$, $K_{iS}$, and $K_{iP}$ are closer than in Figure 3. Although $F_{ei}$ estimate is lower than $F_e$ and y-intercept of Patlak plot, effect on Ki is negligible, likely because in this situation $k_3$ is main determinant of $K_i$ ($k_3$ in this example is three times as high as in Fig. 3). $C_p$ = activity concentration of FDG in plasma; $C_e$ and $C_{ei}$ = region of interest (ROI) concentrations of extravascular FDG serving as substrate pool for hexokinase in Sokoloff and four-compartment models, respectively; $C_{ee}$ = ROI concentration of FDG in extravascular and noncellular compartment; $C_m$ = ROI concentration of phosphorylated FDG.

**A,** Patlak model. $K_{iP}$ = 0.0125/min, *y*-intercept = 0.46 (Patlak equation, $y = 0.0125x + 0.46$). $C_{ROI}$ = $^{18}$F-FDG activity in region of interest.

**B,** Sokoloff model. $K_{iS}$ = 0.0136/min, $k_3$ = 0.0550/min, and $F_e$ = 0.25 ($K_{iS} = k_3 \times F_e$).

**C,** Four-compartment model. $K_{iF}$ = 0.0126/min, $k_3$ = 0.0690/min, $F_{ei}$ = 0.1834, and $F_{ee}$ = 0.1374 ($K_{iF} = k_3 \times F_{ei}$).

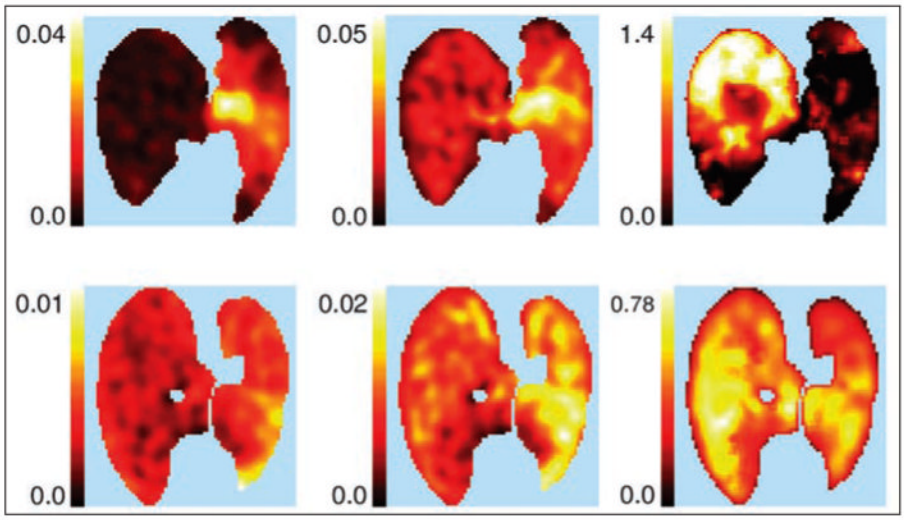


**Fig. 5.**

Sheep exposed to unilateral smoke inhalation. Parametric PET images of ventilation ($10^{-3}$ mL/s) (*left*), Patlak net uptake rate ($K_{iP}$, $min^{-1}$) (*center*), and $K_{iP}$ corrected for tissue fraction ($K_{ip}/F_{tissue}$, $min^{-1}$) (*right*) in two sheep (one in each row) exposed to unilateral smoke inhalation. Smoke-exposed left lung (right side of image) exhibits higher $K_{ip}$ than right (nonexposed) lung, even after correction for lung density. Areas of high $^{18}$F-FDG uptake may correspond not only to alveolar units (*bottom row*) but also central airways (*top row*), as attested by concomitant decrease in ventilation of injured lung. (Reprinted with permission from [80])

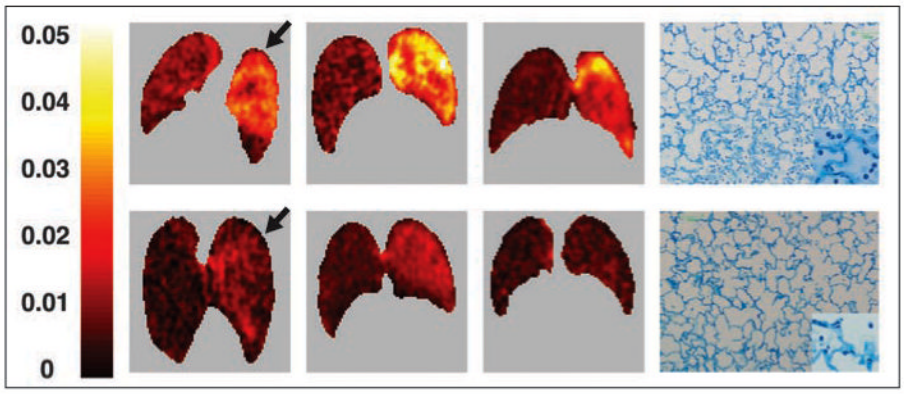


**Fig. 6.**

Three sheep exposed to unilateral ventilator-induced lung injury. Sheep were prone during imaging. Right side of each PET image corresponds to left lung. Parametric images of Patlak net uptake rate ($K_{ip}$) (*three left images*) and lung tissue sections stained with toluidine blue (*right*). In all cases, left lung was subjected to aggressive ventilation strategy involving both alveolar overexpansion and collapse (peak inspiratory pressure, 50 cm $H_2O$; end-expiratory pressure, −10 cm $H_2O$) (*top*) or exclusively alveolar overexpansion (peak inspiratory pressure, 50 cm $H_2O$; end-expiratory pressure, +10 cm $H_2O$) (*bottom*). Right lung was protected from aggressive mechanical ventilation. Arrows indicate lung corresponding to tissue sections displayed on same row. Lung subjected to alveolar overexpansion and collapse (*top*) shows higher $^{18}$F-FDG uptake than does control lung in addition to heterogeneous distribution of aeration with poorly and well-aerated areas, intraalveolar proteinaceous material, and marked cellular infiltration in histologic section. At fourfold higher magnification (*inset*), intraalveolar cells seem to be mainly neutrophils. Lung subjected exclusively to overexpansion (*bottom*) has uniform aeration and some neutrophils. (Reprinted with permission from [35])

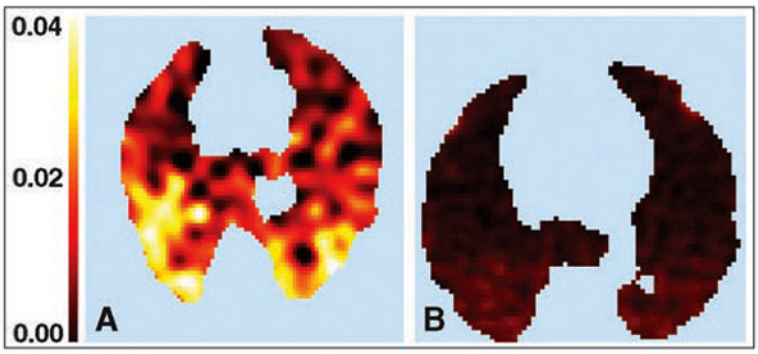


**Fig. 7.**

Sheep exposed and sheep not exposed to two-hit model of acute lung injury. **A** and **B,** Parametric images of Patlak net uptake rate ($K_{iP}$) in two supine sheep exposed (**A**) or not exposed (**B**) to two-hit model of acute lung injury with mild doses of IV endotoxin (10 ng/kg/min for 2 hours) and moderately aggressive mechanical ventilation. $K_{iP}$ is higher in sheep exposed to two-hit injury (color scale is same for **A** and **B**). In addition, distribution of $K_{iP}$ is heterogeneous, being larger in dependent lung regions.

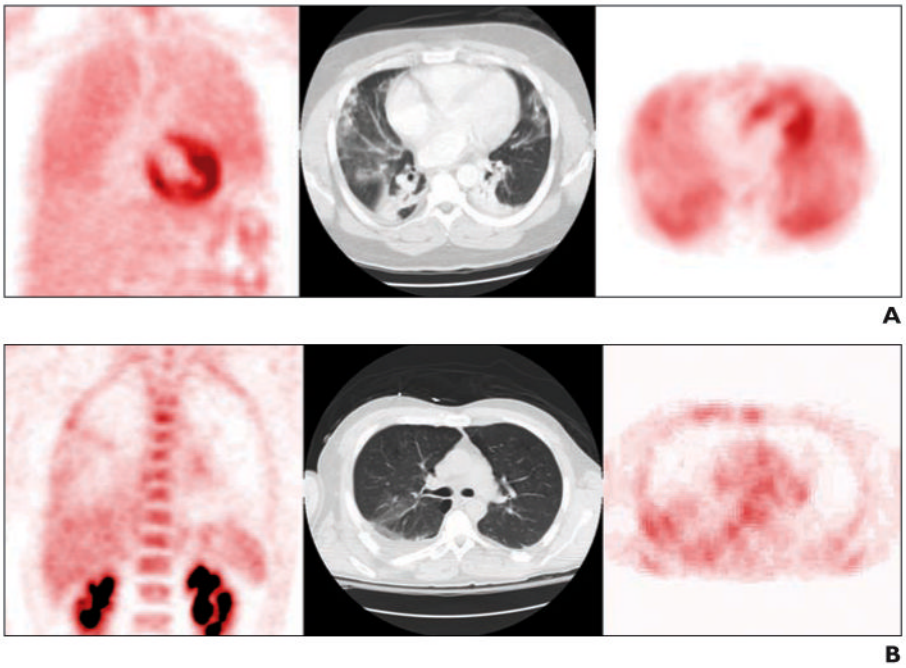


**Fig. 8.**

Patients admitted with thoracic trauma and lung contusion who did not meet criteria for acute respiratory distress syndrome (ARDS) at image acquisition. Coronal $^{18}$F-FDG PET (*left*), transaxial CT image (*center*), and corresponding slice through same region of transaxial PET scan (*right*). (Courtesy of Morton K, University of Utah School of Medicine, Salt Lake City, UT)

**A,** Patient in whom ARDS developed within days after acquisition of these images. FDG PET images show high and diffuse FDG uptake in all portions of lungs, both focally nonaerated and poorly aerated and normally aerated on CT scan.

**B,** Patient in whom ARDS did not develop. FDG PET images show moderate FDG uptake in nonaerated and poorly aerated regions and low FDG uptake in normally aerated regions.